ACS Biomaterials SCIENCE & ENGINEERING

pubs.acs.org/journal/abseba

Article

Gold Nanoparticle-Redox Ionic Liquid based Nanoconjugated Matrix as a Novel Multifunctional Biosensing Interface

Kandaswamy Theyagarajan, Sangeeta Yadav, Jitendra Satija, Kathavarayan Thenmozhi,* and Sellappan Senthilkumar*

Cite This: https://dx.doi.org/10.1021/acsbiomaterials.0c00807

Read Online

ACCESS | Metrics & More | Article Recommendations | Supporting Information

ABSTRACT: Creation of interfaces with a prudent design for the immobilization of biomolecules is substantial in the construction of biosensors for real-time monitoring. Herein, an adept biosensing interface was developed using a nanoconjugated matrix and has been employed toward the electrochemical determination of hydrogen peroxide (H_2O_2). The anionic gold nanoparticle (AuNP) was electrostatically tethered to cationic redox ionic liquid (IL), to which the horseradish peroxidase (HRP) enzyme was covalently immobilized to form a nanobioconjugate. The anthracene-substituted, aldehyde-functionalized redox IL (CHO-AIL) was judiciously designed with the (i) imidazolium cation for electrostatic interaction with AuNPs, (ii) anthracene moiety to mediate the electron transfer, and (iii) free aldehydic group for covalent bonding with a free amine group of the enzyme. Thus, the water-soluble HRP is effectively bonded to the CHO-AIL on a glassy carbon electrode (GCE) via imine bond formation, which resulted in the formation of the HRP-CHO-AIL/GCE. Electrochemical investigations on the HRP-CHO-AIL/GCE reveal highly stable and distinct redox peaks for the anthracene/anthracenium couple at a formal potential ($E^{\circ\prime}$) of −0.47 V. Electrostatic tethering of anionic AuNPs to the HRP-CHO-AIL promotes the electron transfer process in the HRP-CHO-AIL/AuNPs/GCE, as observed by the reduction in the formal potential to −0.42 V along with the enhancement in peak currents. The HRP-CHO-AIL/AuNPs/GCE has been explored toward the electrocatalytic detection of H_2O_2, and the modified electrode demonstrated a linear response toward H_2O_2 in the concentration range of 0.02−2.77 mM with a detection limit of 3.7 μM. The developed biosensor ascertained predominant selectivity and sensitivity in addition to remarkable stability and reproducibility, corroborating the suitableness of the platform for the effectual biosensing of H_2O_2. The eminent performance realized with our biosensor setup is ascribed to the multifunctional efficacy of this newly designed nanobioconjugate.

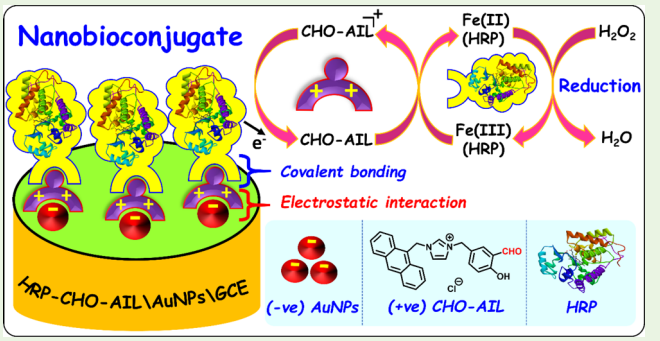

KEYWORDS: *nanobioconjugate, redox ionic liquid, gold nanoparticles, horseradish peroxidase, hydrogen peroxide, electrochemical biosensor*

1. INTRODUCTION

Electrochemical biosensing devices play an integral role in the detection of various significant analytes and are in high demand in healthcare, agriculture, environment, and even in national security. They have gained stupendous importance in the effective determination of target analytes owing to their rapid response time, low cost, simple operation, and high selectivity with good sensitivity.[1−4] These biosensors based on various enzymes, proteins, and antibodies are essentially advantageous in selectively detecting the ultralow concentrations of target analytes in a complex system.[5−7] Despite all these advantages, the efficacy of these biosensors critically relies on (i) stable immobilization and suitable orientation of biomolecules and (ii) communication between the electroactive prosthetic group in the biomolecule and electrochemical transducers.[8,9] Various redox mediators, nanomaterials, and conducting polymers are being incorporated in the electrode setup for surmounting these challenges.

Redox mediators such as azure A, ferrocene, neutral red, thionine, and toluidine blue are mostly being utilized for shuttling the electrons between the electrode and the enzyme molecules.[10−12] Meanwhile, noble metal nanoparticles have emerged as promising materials owing to their distinguished sensitivity that arises from the increased surface area, excellent surface-to-volume ratio, and intrinsic electronic properties.

Received: May 27, 2020
Accepted: October 8, 2020

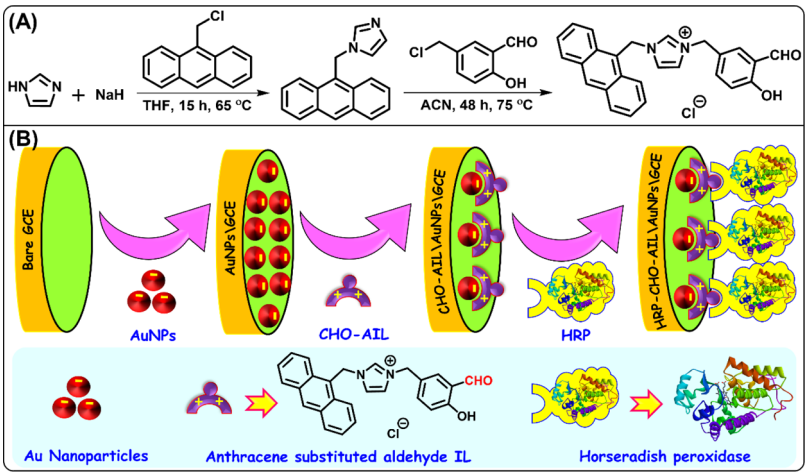

Figure 1. (A) Schematic illustration of the synthesis of anthracene-substituted aldehyde IL (CHO-AIL). (B) Step-wise fabrication of the HRP-CHO-AIL/AuNPs/GCE.

Especially, the gold nanoparticles (AuNPs) are of high interest in electroanalytical applications because of their distinctive electrochemical characteristics and ease of synthesis with tailor-made protecting groups.[13,14] Several reports on AuNPs suggest that these can be exploited to create an effective electrochemical interface for various enzymatic reactions.[15−17] However, most of these platforms were unable to retain all the essential qualities of biomolecules to be developed into a biosensor, especially to hold or preserve the nativity and functionality of the enzymes, which could considerably affect the stability of the fabricated biosensors. This inspired us to develop a highly versatile and facile sensor matrix that can provide stable anchoring of biomolecules, along with efficacy to preserve the enzyme's nativity and further expedite the electron shuttle between the electrode and biomolecule.

Ionic liquids (ILs) are considered to be exceptionally promising candidates in diverse and thrust areas of research including batteries, supercapacitors, solar cells, catalysis, and sensors and biosensors owing to their fascinating characteristics, which include wide electrochemical potential window, low volatility, enhanced thermal stability, and nontoxicity.[18−21] In particular, their typical properties of high conductivity and good biocompatibility are of immense interest in bioelectronics for establishing a meaningful bridge between the enzymes and electrochemical probes. Furthermore, ILs offer outstanding synthetic versatility and these molecules can be judiciously tuned with an appropriate choice of cations (imidazolium, phosphonium, pyridinium, etc.) and anions (inorganic to organic) to suit distinct applications based on the requirement. ILs comprising different functional groups such as $-NH_2$, $-COOH$, $-CHO$, $-OH$, $-SO_3H$, and so on have been designed for accomplishing various task-specific applications.[22−26] Taking all these merits associated with ILs into account, we intended to design and synthesize a novel IL-based biosensing interface with multiple efficacies such as facile immobilization of biomolecules, efficient electrical communication through a redox mediator, larger surface area, and high electronic conductivity. AuNPs were chosen to afford a high surface area and conductivity and could be electrostatically tethered to the cationic part of ILs. In addition, the IL could be designed as redox-active via suitable substitution to facilitate the electrical communication for effectual biosensing. Since we have obtained promising performance with the aldehyde-functionalized IL for immobilization of glucose oxidase enzymes and detection of glucose in our previous work,[26] we sought to leap ahead with an analogous aldehyde functional group for the covalent immobilization of biomolecules in the present investigation. Horseradish peroxidase (HRP) has been adopted to serve as a model biomolecule to demonstrate the versatility of the newly developed platform. HRP is a metalloenzyme containing a heme group extracted from the roots of horseradish and the widely utilized enzyme in the fabrication of biosensors for the determination of hydrogen peroxide (H_2O_2).[27,28] Qualitative and quantitative determination of H_2O_2 is a highly crucial and persuasive process needed in food processing, pharmaceutical industry, pulp and textile bleaching, clinical diagnosis, and environmental monitoring.[29−31] Thus, the establishment of highly reliable analytical tools and methodologies toward selective and sensitive determination of H_2O_2 remains the need of the hour.[32]

Herein, we have prudently framed a nanoconjugated matrix using an anthracene-substituted, aldehyde-functionalized cationic redox IL (CHO-AIL) electrostatically tethered to anionic AuNPs on the GCE as a befitting scaffold toward covalent anchoring of the HRP enzyme and utilized it for selective biosensing of H_2O_2. The platform comprises a free aldehyde group to covalently anchor the HRP enzyme via imine bond formation and anthracene group in the IL form, which serves as the redox mediator. Furthermore, negatively charged AuNPs have been prepared exclusively to facilitate them to be electrostatically tethered to the bulky positive charge on the CHO-AIL. A facile electron transfer was achieved by the anthracene/anthracenium redox couple, and a stable enzyme immobilization was obtained because of the covalent anchoring with impressive biocompatibility and synthetic versatility offered by the CHO-AIL. Electrostatic incorporation of AuNPs provided a biosensing interface with the enhanced surface area for the CHO-AIL and good electronic conductivity for the rapid shuttling of electrons, which ultimately augmented the biosensor performance.

2. EXPERIMENTAL SECTION

2.1. Chemicals and Reagents. 9-(Chloromethyl)anthracene (≥98%), imidazole (≥99%), sodium hydride (60% dispersion in mineral oil), salicylaldehyde (≥98%), formaldehyde (37%), and

https://dx.doi.org/10.1021/acsbiomaterials.0c00807
ACS Biomater. Sci. Eng. XXXX, XXX, XXX−XXX

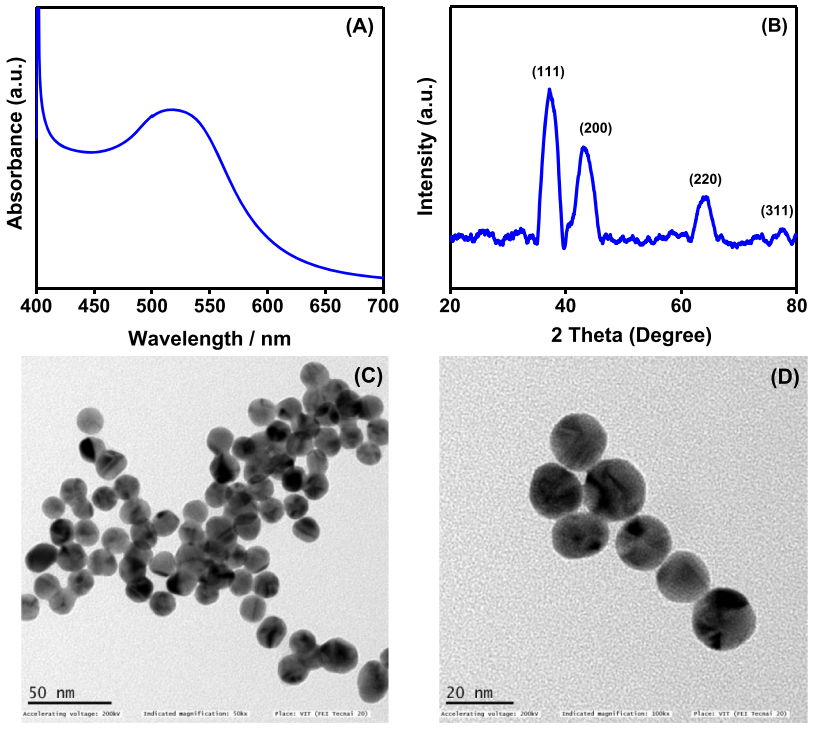

Figure 2. (A) UV−vis absorption spectrum, (B) XRD, and (C,D) TEM images of AuNPs.

gold(III) chloride ($HAuCl_4$) (99.99%, 30 wt % in dilute HCl) were bought from Sigma-Aldrich (India). H_2O_2 (30%) was obtained from Merck (India). Sodium citrate tribasic dihydrate (TSC) and HRP were procured from Sisco Research Laboratories (India). Other common chemicals were employed as obtained (analytical grade) without additional treatment. Milli-Q water (resistivity: 18.2 MΩ cm at 25 °C) was used to prepare all the aqueous solutions. Monosodium and disodium phosphate salts were used for preparing the phosphate buffer, and aqueous sodium hydroxide and hydrochloric acid solutions were used to adjust pH. All glassware used for nanoparticle synthesis and storage were thoroughly precleaned with aqua regia ($3HCl:1HNO_3$).

2.2. Instrumentation. Nuclear magnetic resonance (NMR) spectral analysis was performed on a Bruker Ascend spectrometer (400 MHz) using $CDCl_3$/DMSO-d_6 as the solvent, and the chemical shift (δ) values are presented in ppm and referred to tetramethyl silane (δ = 0.00). A Shimadzu IR Affinity-1 spectrophotometer was used for recording the Fourier-transform infrared (FTIR) spectra using an attenuated total reflectance method over the range of 4000 to 400 cm^{-1}. A JASCO V-670 spectrophotometer was used for UV−visible (UV−vis) spectral analysis with a path length (l) of 1 cm. An FEI-Tecnai G2 20 Twin (200 kV) was used for high-resolution transmission electron microscopy (HR-TEM). A D8 ADVANCE (Bruker) diffractometer with a monochromatic source (Cu Kα radiation, λ = 1.5418 Å) was used to study the X-ray diffraction (XRD) pattern. A JEOL GC Mate-II spectrometer with electron impact ionization (70 eV) was used for recording the high-resolution mass spectra (HRMS). The electrochemical experiments such as amperometry and cyclic voltammetry (CV) were performed with a CHI760E (CH Instruments, USA) electrochemical workstation, and the impedance measurements were conducted in an Autolab PGSTAT204 (Metrohm Autolab, Netherlands) potentiostat. These electrochemical experiments were carried out in a regular three-electrode cell comprising (i) an unmodified/modified glassy carbon electrode (GCE) as the working electrode, (ii) an aqueous Ag/AgCl (3 M KCl) as a reference, and (iii) a platinum spiral as the counter electrode. All electrochemical experiments were performed in a deoxygenated buffer solution under a nitrogen atmosphere (inert).

2.3. Synthesis of Anthracene-substituted Aldehyde-functionalized IL. An anthracene-substituted aldehyde-functionalized IL was synthesized by the steps as shown in Figure 1A.

2.3.1. Synthesis of 1-Anthracene-9-ylmethylimidazole. A 21 mmol of sodium hydride (oil free) was stirred in dry THF at an ice-cold condition. To this stirred solution, 20 mmol of imidazole solution in dry THF was added slowly. Thereafter, an ice bath was removed and stirring continued for 1 more hour at room temperature (RT). Subsequently, 20 mmol of 9-(chloromethyl)anthracene in dry THF was supplemented to this mixture and refluxed for 15 h at 65 °C. Afterward, the solid residue was filtered out and THF was removed by a rotary evaporator. The resulting residue was thoroughly washed using water and then extracted using chloroform. The collected extract was subjected to drying over magnesium sulphate (anhydrous), and chloroform was evaporated to obtain 1-(anthracene-9-ylmethyl)-imidazole as a yellow solid (92% yield). ^{1}H NMR (400 MHz, $CDCl_3$): δ 6.01 (s, 2H, $-CH_2-$), 6.85 (s, 1H), 7.00 (s, 1H), 7.47−7.56 (m, 5H), 8.04−8.06 (d, 2H), 8.15−8.17 (d, 2H), 8.53 (s, 1H) ppm. ^{13}C NMR (100 MHz, $CDCl_3$): δ 43.07, 118.93, 123.0, 124.71, 125.34, 127.39, 129.38, 129.50, 130.80, 131.45, 136.85 ppm (Figure S1).

2.3.2. Synthesis of 1-(Anthracene-9-ylmethyl)-3-(3-formyl-4-hydroxybenzyl)-imidazol-3-ium Chloride (CHO-AIL). 5-Chloromethyl-2-hydroxybenzaldehyde (15 mmol) in acetonitrile was added gradually to an acetonitrile (35 mL) solution of 1-(anthracene-9-ylmethyl)-1*H*-imidazole (15.1 mmol) under stirring. This mixture was refluxed at 75 °C for 48 h, after which it was cooled to RT and the solid was separated. The residue was thoroughly washed using diethyl ether, followed by vacuum drying to obtain CHO-AIL as a pale-yellow solid (91% yield). ^{1}H NMR (400 MHz, DMSO-d_6): δ 5.25 (s, 2H, $-CH_2-$), 6.49 (s, 2H, $-CH_2-$), 7.07−7.09 (d, 1H), 7.49−7.52 (m, 1H), 7.59−7.69 (m, 6H), 7.73−7.74 (t, 1H), 8.21−8.23 (d, 2H), 8.44−8.46 (d, 2H), 8.84 (s, 1H), 9.18 (s, 1H), 10.26 (s, 1H, −CHO), 11.13 (s, 1H, −OH) ppm. ^{13}C NMR (100 MHz, DMSO-d_6): δ 45.47, 51.55, 118.53, 122.85, 122.94, 123.35, 123.84, 123.95, 126.08, 126.13, 128.25, 128.93, 129.88, 130.61, 131.09, 131.54, 136.15, 136.81, 161.69, 190.58 ppm. HRMS (EI): $[C_{26}H_{21}N_2O_2]^+$ calcd, 393.4655; found, 393.4652 (Figures S2 and S3).

2.4. Synthesis of Negatively Charged AuNPs. In order to form the nanoconjugate of ILs with AuNPs, we intended to prepare

https://dx.doi.org/10.1021/acsbiomaterials.0c00807
ACS Biomater. Sci. Eng. XXXX, XXX, XXX−XXX

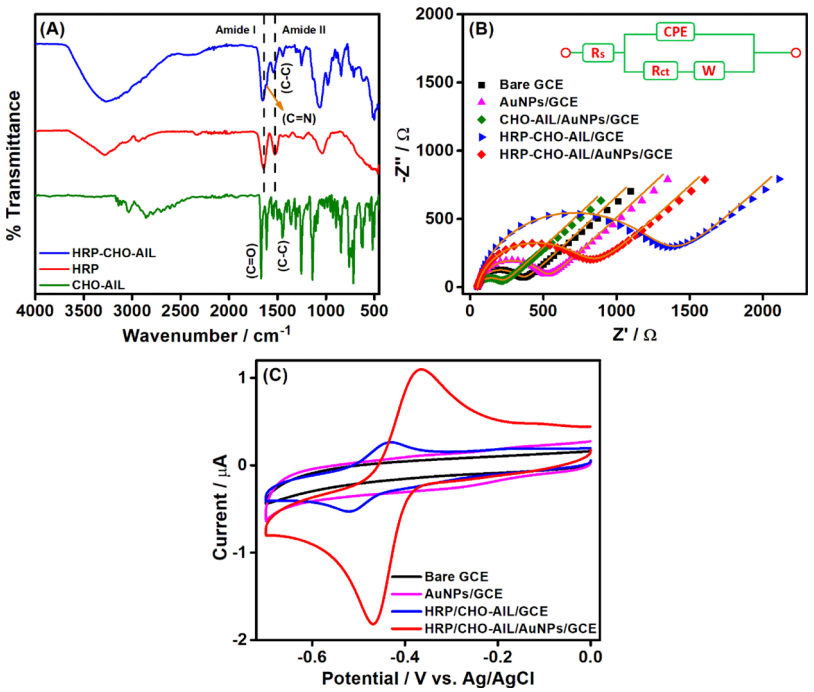

Figure 3. (A) Comparative FTIR spectra of CHO-AIL (green), HRP (red), and HRP-CHO-AIL (blue). (B) Nyquist plots of the unmodified GCE (black), AuNPs/GCE (pink), CHO-AIL/AuNPs/GCE (green), HRP-CHO-AIL/GCE (blue), and HRP-CHO-AIL/AuNPs/GCE (red) in a 0.1 M KCl electrolyte with 2.5 mM of $[Fe(CN)_6]^{3-/4-}$ (inset: equivalent circuit used to fit EIS data), and (C) CVs of the unmodified GCE (black), AuNPs/GCE (pink), HRP-CHO-AIL/GCE (blue), and HRP-CHO-AIL/AuNPs/GCE (red) measured in phosphate buffer (0.1 M, pH 7.0) at a sweep rate of 50 mV/s.

negatively charged nanoparticles, following the procedure reported in the literature with minor modification.[33] Briefly, a 50 mL aqueous solution of $HAuCl_4$ (1 mM) was heated to boiling temperature under the vigorous stirring condition. This was followed by the quick addition of a 5 mL of TSC solution (38.8 mM). The resulting mixture was boiled for an additional 20 min, which turned the pale-yellow solution to deep red, confirming the formation of stable AuNPs. This colloidal solution was cooled to RT and preserved in a refrigerator at 4 °C.

2.5. Fabrication of the HRP-CHO-AIL/AuNPs/GCE Biosensor. Initially, a GCE was mirror-polished on a cloth pad with alumina slurries (1.00, 0.30, and 0.05 μm) successively, sonicated for 5 min in the ethanol/H_2O (1:1 v/v) mixture, and then dried in the open air. This mirror-polished GCE was coated with 5 μL of anionic AuNPs and allowed to dry at RT to form a negatively charged AuNP surface over the GCE (AuNPs/GCE). Then, 5 μL of cationic CHO-AIL (1 mg/50 μL of MeOH) was drop-casted over the AuNPs/GCE to form a stable electrostatically attracted CHO-AIL/AuNPs/GCE. Furthermore, 5 μL of HRP solution (10 mg/mL) was drop-casted over the CHO-AIL/AuNPs/GCE and incubated (2 h) to form a stable imine linkage between the free $-NH_2$ functional group of enzymes and −CHO functionality of CHO-AIL through Schiff base condensation. Afterward, the fabricated electrode was repeatedly washed with phosphate buffer to remove any loosely bound or nonbonded HRP from the sensor matrix, giving rise to the HRP-CHO-AIL/AuNPs/GCE. The step-wise construction of the proposed biosensor is displayed in Figure 1B. For comparison, another electrode was constructed without employing AuNPs in the sensor matrix and is referred to as HRP-CHO-AIL/GCE.

3. RESULTS AND DISCUSSION

3.1. Characterization of Gold Nanoparticles. The absorption spectrum of the as-prepared AuNPs shows the characteristic localized surface plasmon resonance peak at around 517 nm, indicating the generation of nanoparticles with uniform size distribution (Figure 2A). The XRD analysis of AuNPs, drop-casted on a glass coverslip, revealed the typical peaks at 37.54, 43.86, 64.01, and 77.55 ascribed to 111, 200, 220, and 311 crystal planes of AuNPs, respectively, which are in agreement with the data reported in JCPDS 00-001-1172 (Figure 2B). The TEM image analysis corroborates the UV−visible spectroscopic results and shows the generation of spherical AuNPs with an average size of 15.65 ± 1.80 nm (Figure 2C,D). The hydrodynamic size measured by dynamic light scattering was found to be 34.39 ± 0.64 nm. Furthermore, the zeta potential of AuNPs was estimated to be −65.76 ± 13.23 mV, which clearly evidences the presence of negative charges at the AuNP surface by virtue of TSC as the capping agent.[34,35]

3.2. Spectral Investigation of HRP-CHO-AIL. The covalent attachment of HRP on CHO-AIL through the formation of a strong imine bond was confirmed by investigations using FTIR spectra. The samples for FTIR spectra were obtained by scratching off the fabricated electrode surface with a custom-made needle, followed by drying and recording of the spectra using the ATR mode. In Figure 3A, the green curve represents the FTIR spectrum of CHO-AIL, which shows a sharp band at 1664 cm^{-1} representing the aldehydic (C═O) stretching frequency of terminal aldehyde groups, and peaks around 2850 and 1450 cm^{-1} correspond to stretching frequencies of aromatic C−H and C−C bonds, respectively.[36,37] The red curve represents the HRP enzyme, which illustrates typical stretching frequencies for amide I and amide II around 1646 and 1525 cm^{-1}, respectively.[38] The blue curve denotes the FTIR spectrum of covalently immobilized HRP on CHO-AIL, which was confirmed through the absence of aldehydic (C═O) stretching (1664 cm^{-1}) frequency and advent of C═N stretching frequency at 1612 cm^{-1}, which appears as a shoulder peak with an amide I band of HRP.[37]

https://dx.doi.org/10.1021/acsbiomaterials.0c00807
ACS Biomater. Sci. Eng. XXXX, XXX, XXX−XXX

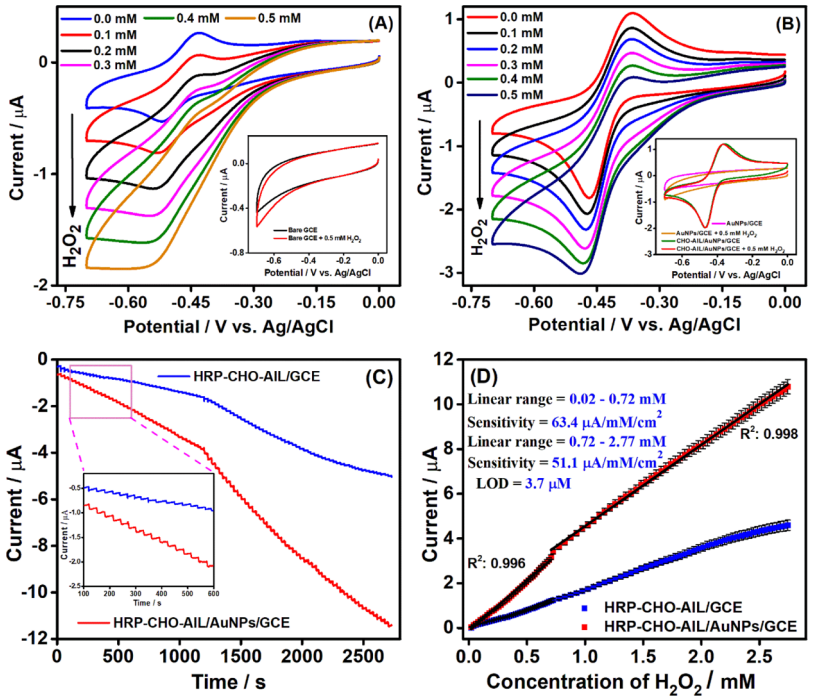

Figure 4. (A) CVs of the HRP-CHO-AIL/GCE and (B) CVs of the HRP-CHO-AIL/AuNPs/GCE with increasing concentrations of H_2O_2 at 50 mV/s. Insets: CVs of the (A) unmodified GCE and (B) AuNPs/GCE and CHO-AIL/AuNPs/GCE in the presence (0.5 mM) and absence of H_2O_2. (C) Amperometric response for the successive spikes of H_2O_2 under constant stirring (350 rpm) at −0.45 V and (D) corresponding calibration plot.

Furthermore, both the amide peaks of HRP were preserved in HRP-CHO-AIL, which suggests that the enzyme preserves its native state even after being covalently bonded to CHO-AIL. These results confirm the establishment of a covalent linkage between HRP and CHO-AIL and also the retainment of the native state of the enzyme in the immobilized form, which is attributed to the virtuous biocompatibility offered by CHO-AIL.

3.3. Electrochemical Impedance Measurements on the HRP-CHO-AIL/AuNPs/GCE. Electrochemical impedance spectroscopy (EIS) aids in investigating the interface by following the change in impedance between the electrolyte and electrode interface during step-wise fabrication of the biosensor. The Nyquist plot from EIS exhibits a semicircle in the high-frequency range, and the diameter of this semicircle represents the charge transfer resistance (R_{ct}). Figure 3B shows the EIS results obtained for the electrodes in a 0.1 M KCl electrolyte with 2.5 mM $[Fe(CN)_6]^{3-/4-}$, and these results were fitted using the Randle's circuit [Figure 3B (inset)]. The unmodified GCE exhibited a R_{ct} of 309 Ω, representing a sluggish redox behavior; however, after drop-casting AuNPs on the GCE (AuNPs/GCE, pink curve), the R_{ct} increased to 486 Ω. This is attributed to the repulsion between the $[Fe(CN)_6]^{3-/4-}$ anions present in the solution and the negatively charged AuNP/GCE surface, which confirms that the anionic AuNPs were effectively immobilized over the GCE surface.[39] After immobilization of CHO-AIL on the AuNPs/GCE (CHO-AIL/AuNPs/GCE, green curve), the negative charge in AuNPs is compensated by the positively charged ions in the CHO-AIL and the electrostatic repulsion observed with $[Fe(CN)_6]^{3-/4-}$ is remarkably subsided. Thus, a very low R_{ct} of 163 Ω was observed for the CHO-AIL/AuNPs/GCE, which is ascribed to high conductivity afforded by the CHO-AIL/AuNPs matrix. Nevertheless, covalent attachment of HRP on the CHO-AIL/GCE (HRP-CHO-AIL/GCE, blue curve) increases the R_{ct} of the modified electrode to the highest value of 1336 Ω, which confirms the firm anchoring of the nonconducting biomolecule on the surface.[40] Furthermore, incorporation of AuNPs (HRP-CHO-AIL/AuNPs/GCE, red curve) in the biosensor matrix significantly reduces the R_{ct} to 795 Ω. The EIS outcomes imply that the fabricated CHO-AIL/AuNPs/GCE nanoconjugate-based sensing interface provided an enhanced conductivity, which expedited the fast electron transfer between the electrode and active sites of the covalently immobilized biomolecules.

3.4. Electrochemical Investigations on the HRP-CHO-AIL/AuNPs/GCE. The electrochemical response of the HRP-CHO-AIL/AuNPs/GCE was examined sequentially with CV in N_2 satd. phosphate buffer (0.1 M, pH 7.0) within the potential window of 0.0 and −0.7 V at a sweep rate of 50 mV/s (Figure 3C). No apparent redox signals were observed for the unmodified GCE and AuNPs/GCE within the given potential window. Immobilization of HRP on the AuNPs modified GCE (without CHO-AIL) resulted in a highly unstable and inconsistent CV response (figure not shown). However, the HRP-CHO-AIL/GCE showed a well-resolved and stable redox peak for the anthracene/anthracenium couple with anodic (E_{pa}) and cathodic (E_{pc}) peak potentials at −0.43 and −0.52 V, respectively.[41,42] A distinct redox peak with enhanced redox peak currents was obtained in the case of the HRP-CHO-AIL/AuNPs/GCE with an E_{pa} value of −0.37 V and an E_{pc} value of −0.47 V. Moreover, a less formal potential ($E^{o\prime}$) of −0.42 V was obtained with the HRP-CHO-AIL/AuNPs/GCE compared to that of HRP-CHO-AIL/GCE ($E^{o\prime}$ −0.47 V) with an increased peak current, which is attributable to the highly conductive nature of AuNPs with the enhanced surface area along with the electrostatically tethered redox-active CHO-AIL to the fabricated biosensor.

https://dx.doi.org/10.1021/acsbiomaterials.0c00807
ACS Biomater. Sci. Eng. XXXX, XXX, XXX−XXX

Table 1. Comparative Performances of Enzyme-based H_2O_2 Biosensors

biosensors	linear range (mM)	sensitivity (μA mM^{-1} cm^{-2})	LOD (μM)	ref.
HRP-OANW	0.02−0.5	31	5	43
HRP-OANP	0.02−0.5	27	8	43
GCE/CtRGO/PAMAM/GA/HRP	0.05−0.8	29.86	25	44
GCE/PAMAM/GA/HRP	0.2−1.1	5.68	50	44
GCE/GA/5%Pt NPs/Cyt c	0.005−1.175	5.3	1.67	45
Hb−AgNPs-PAMAM/GCE	0.006−0.09		4.9	46
HRP/LDH-CMC/GCE	0.02−6.0	220	12.4	47
PCS/Hb/CPE	0.1−5.0	76.43	32	48
Hb-CB-ZE/GCE	0.004−0.39		4.0	49
HRP-CHO-AIL/AuNPs/GCE	0.02−0.72	63.4	3.7	this work
	0.72−2.77	51.1		

Furthermore, the electroactive surface areas of the unmodified GCE, AuNPs/GCE, and CHO-AIL/AuNPs/GCE were calculated using Randles−Sevick eq 1

$$I_p = (2.69 \times 10^5) D^{1/2} A n^{3/2} C v^{1/2} \quad (1)$$

where I_p is the peak current (A), D is the diffusion coefficient of the species (cm^2 s^{-1}), C is the concentration of the species in solution (mol L^{-1}), A is the electroactive surface area (cm^2), n is the number of electrons transferred, and v is the sweep rate (V s^{-1}). The electroactive surface areas of various modified electrodes were estimated to be 0.042 cm^2 for the unmodified GCE, 0.122 cm^2 for AuNPs/GCE, and 0.139 cm^2 for CHO-AIL/AuNPs/GCE. It could be noticed that the introduction of AuNPs has strikingly increased the electroactive area, and CHO-AIL/AuNPs/GCE has shown 3.3 times increase in the surface area than that of unmodified GCE, which in turn would assist better immobilization and orientation of HRP in the developed sensor. The influence of pH of the electrolyte on the fabricated biosensor was probed by performing CVs in phosphate buffers of different pH values, ranging between 6 and 10, at a sweep rate of 50 mV/s (Figure S4A). When the pH was increased from 6 to 10, the redox peak potentials were shifted to the more negative region and the plot of peak potentials versus pH resulted in a linear trend with a slope of 63 mV/pH (Figure S4B), which is closer to the Nernstian behavior of 59 mV/pH for one proton coupled with one electron transfer. Moreover, a maximum peak current was achieved at the neutral pH and hence pH 7.0 was chosen for probing the electrocatalytic activity. Furthermore, the influence of the sweep rate on the developed HRP-CHO-AIL/AuNPs/GCE was examined by increasing the sweep rate between 5 and 120 mV/s, which is shown in Figure S5. On increasing the sweep rate, the cathodic and anodic peak currents show an increase with a feeble shift in the peak potential and the plot of peak currents versus square root of the sweep rate depicts a linear relationship, corresponding to a diffusion-controlled redox process.

3.5. Electrocatalytic Behavior of the HRP-CHO-AIL/AuNPs/GCE for H_2O_2 Reduction. After the successful characterization of the fabricated biosensor by EIS and CV, the electrocatalytic efficacy of the nanobioconjugate toward H_2O_2 reduction was probed using CV. Figure 4A displays the CVs obtained for the sequential additions of H_2O_2 in phosphate buffer (N_2 satd., 0.1 M, pH 7.0) at a sweep rate of 50 mV/s using the HRP-CHO-AIL/GCE. For every incremental addition of the analyte, there was an immediate increase in the reduction current, along with a subsequent decline in the oxidation current, implying the electrocatalytic H_2O_2 reduction. The nanoconjugated matrix-based HRP-CHO-AIL/AuNPs/GCE (with AuNPs) showed a significantly higher catalytic current response with a less onset potential than the HRP-CHO-AIL/GCE (without AuNPs) for the same concentrations of H_2O_2 (Figure 4B). The increase in the reduction current varied linearly with the amount of H_2O_2 spiked into the electrolyte solution, which confirms that the HRP-CHO-AIL/GCE could effectively reduce H_2O_2. The higher catalytic current with a less formal potential observed for the HRP-CHO-AIL/AuNPs/GCE is due to the improved electronic conductivity and vast electroactive surface provided by AuNPs along with the electrostatically tethered biocompatible CHO-AIL. Instead, the unmodified GCE (Figure 4A, inset), AuNPs/GCE (Figure 4B, inset), and CHO-AIL/AuNPs/GCE (Figure 4B, inset) displayed an ineffectual response for even 0.5 mM H_2O_2 under similar conditions. Thus, effective communication with the heme active site of HRP was realized in this nanostructured multifunctional interface through the electrical wiring made over the new redox-active CHO-AIL and AuNPs, which makes the fabricated electrode a stable biosensor for the effective determination of H_2O_2.

After studying the electrocatalytic activity of the HRP-CHO-AIL/AuNPs/GCE toward H_2O_2 in a static condition, the competence of the developed electrode was verified using amperometry in dynamic conditions (Figure 4C). Amperometry was performed with the HRP-CHO-AIL/GCE and HRP-CHO-AIL/AuNPs/GCE in a stirred phosphate buffer (N_2 satd., 0.1 M, pH 7.0). Initially, the operating potential for the amperometric studies was optimized by carrying out the measurements at increasing potentials between −0.35 and −0.55 V (Figure S6). Upon increasing the operating potentials, the current response of the HRP/CHO-AIL/AuNPs/GCE toward H_2O_2 determination was also found to increase up to −0.45 V. Though a slightly higher current was obtained beyond −0.45 V, the current response was not linear at very high potentials, and hence, −0.45 V was selected as the optimal voltage for amperometric H_2O_2 detection. For every incremental addition of H_2O_2 with HRP-CHO-AIL/AuNPs/GCE at −0.45 V, we observed an immediate increase in the current response and this gets stabilized in <3 s and attains a steady state. However, a less catalytic current with a nonlinear response was observed for the HRP-CHO-AIL/GCE, which shows that the AuNPs with intrinsic conductivity in the nanoconjugated matrix afford enhanced sensitivity. The favorable microenvironment of HRP in the CHO-AIL matrix with the fast electron shuttling of the anthracene mediator along with AuNPs synchronously contributes to the quick

https://dx.doi.org/10.1021/acsbiomaterials.0c00807
ACS Biomater. Sci. Eng. XXXX, XXX, XXX−XXX

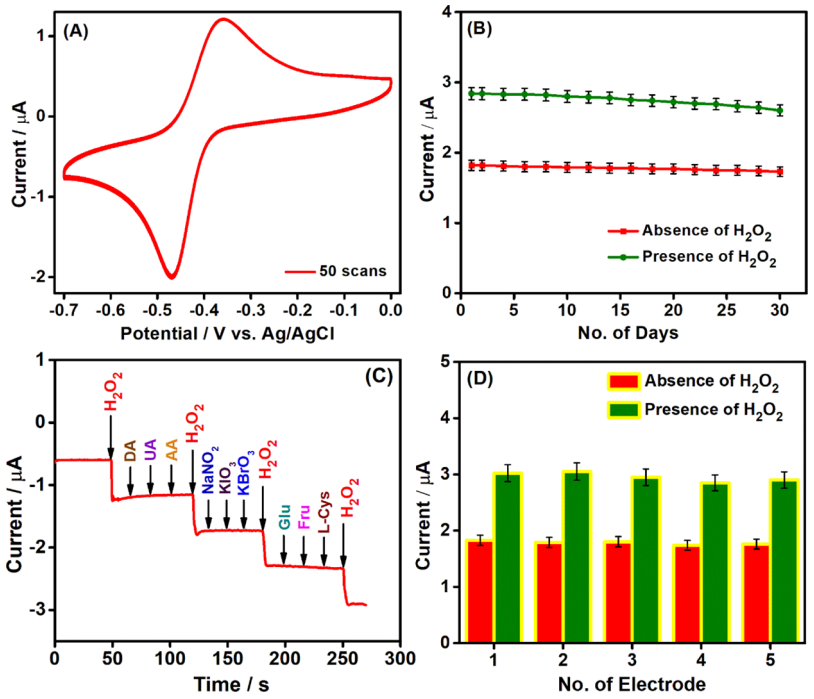

Figure 5. (A) Effect of potential scans for 50 continuous cycles, (B) long-term stability for 30 days in the presence (0.4 mM) and absence of H_2O_2, (C) effect of interference by performing amperometry toward H_2O_2 addition (0.15 mM) in the presence of various interfering agents (1 mM) in a stirred phosphate buffer (0.1 M, pH 7.0), and (D) current response bar diagram in the presence (0.5 mM) and absence of H_2O_2 for five similarly prepared biosensors.

catalytic response. On plotting the catalytic current versus H_2O_2 concentration (Figure 4D), it varied linearly but in two concentration ranges from 20 μM to 0.72 mM and 0.72 mM to 2.77 mM with sensitivities of 63.4 and 51.1 μA mM^{-1} cm^{-2} and a limit of detection of 3.7 μM. Thus, the nanobioconjugate-based sensing interface offered promising results toward the sensitive determination of H_2O_2. The overall performance of the nanoconjugated matrix-derived biosensor toward H_2O_2 determination was compared with the published literature, and it is clear that the fabricated biosensor exhibited a comparable or better electrocatalytic response compared to previous reports (Table 1).

3.6. Stability, Selectivity, and Reproducibility. An essential requirement of a biosensing interface is to provide a stable and reproducible response for a longer time. Accordingly, the fabricated biosensor was tested for its stability by subjecting it to 50 continuous scans at a sweep rate of 50 mV/s in phosphate buffer (0.1 M, pH 7.0), as shown in Figure 5A. Noticeably, no significant variation in the peak currents as well as in peak potentials was observed, which implies the enhanced cyclic stability of the HRP-CHO-AIL/AuNPs/GCE. Furthermore, the biosensor was examined for the long-term storage stability for 30 long days, and it was found that the biosensor could retain 95% of the original current in the absence of H_2O_2 and 92% in the presence of 0.4 mM H_2O_2 (Figure 5B). The enhanced cyclic stability with acceptable storage stability was accredited to the firm covalent attachment of HRP on a CHO-AIL/AuNPs based biocompatible and highly conducting nanoconjugated matrix. In the electrode design, the biosensing interface not only performs a pivotal role as a quick electron shuttle but also serves as a host and anchoring site to retain the nativity and stability of the highly sensitive HRP enzyme. The HRP-CHO-AIL/AuNPs/GCE displayed stable and consistent voltammograms only in the pH range between 6 and 10 (Figure S4), and the voltammetric response was not stable under a strongly acidic or basic environment. We are uncertain at this moment whether the unstable CV response at strong acidic/basic conditions is due to the instability of the imine bond or denaturation of the enzyme. The fabricated biosensor was preserved in a refrigerator at 4 °C after each experiment.

The selectivity of the HRP-CHO-AIL/AuNPs/GCE was evaluated by adding some commonly interfering electroactive species. Figure 5C depicts the amperometric current response acquired for 0.15 mM of H_2O_2 along with 1 mM of electroactive and commonly co-existing compounds like uric acid, dopamine, ascorbic acid, sodium nitrite, potassium iodate, potassium bromate, glucose, fructose, and L-cysteine in a continuously stirred electrolyte. Impressively, the fabricated biosensor showed a catalytic current response only on H_2O_2 addition and no significant signal was noticed for other interfering species, which indicates its high selectivity. Furthermore, the reproducibility of the developed biosensor was tested by preparing five different HRP-CHO-AIL/AuNPs/GCEs by following similar protocols, and their catalytic current response toward 0.5 mM H_2O_2 was analyzed, as shown in Figure 5D. The relative standard deviation (RSD) values were found to be 2.8 and 1.98% in the presence and absence of H_2O_2, respectively, which indicates the acceptable electrode-to-electrode reproducibility of the constructed electrode.

3.7. Real-Sample Analysis. The practical usability of the fabricated biosensor was tested by quantifying H_2O_2 in real-world samples like apple juice, milk, and goat serum. The amperometric determination was performed with known concentrations of H_2O_2 spiked in the diluted real samples. The fabricated HRP-CHO-AIL/AuNPs/GCE was adept in estimating the concentrations of H_2O_2 with the recoveries ranging from 97.8 to 102.1% with an acceptable RSD (Table

https://dx.doi.org/10.1021/acsbiomaterials.0c00807
ACS Biomater. Sci. Eng. XXXX, XXX, XXX−XXX

2). These observations ensure that the fabricated electrode is suitable toward sensing of H_2O_2 in real-life samples, and this is ascribed to the excellent sensitivity and selectivity originated from the stable immobilization of HRP on the newly developed nanoconjugated matrix.

Table 2. Determination of H_2O_2 Spiked into Various Real-Life Samples

real sample	spiked (mM)	mean found (mM)	recovery (%)	RSD[a] (%)
apple juice	0.3	0.295	98.3	2.3
	0.6	0.613	102.1	2.7
milk	0.4	0.405	101.2	2.5
	0.8	0.802	100.2	1.9
goat serum	0.5	0.489	97.8	2.6
	1.0	1.011	101.1	2.2

[a]Triplicates were performed.

4. CONCLUSIONS

In summary, a nanostructured matrix was designed to be a novel interface toward effective covalent anchoring of HRP. The biosensing interface comprises a conjugate of anthracene-substituted aldehyde-functionalized cationic redox IL electrostatically tethered to a negatively charged AuNPs. CHO-AIL facilitated the covalent immobilization of the HRP enzyme with its aldehyde group, and the anthracene group of this redox IL effectively mediated the electron shuttling across the deeply buried redox-active center of HRP and the electrode surface. Furthermore, AuNPs along with CHO-AIL synchronously enhanced the conductivity, which significantly augmented the biosensing. This multifunctional nanobioconjugate-based biosensor thus obtained provided promising performances, pertaining to electrocatalytic activity, selectivity, sensitivity, reproducibility, and stability toward effective determination of H_2O_2. The enhanced sensing parameters of the biosensor could be ascribed to the effectual bonding of enzymes on this biocompatible and conductive CHO-AIL/AuNPs platform. Thus, the nanoconjugate-derived matrix reported here could open new and interesting opportunities toward the fabrication of various biosensors and immunosensors and also could shed light on the development of tailor-made platforms for a wide variety of applications.

■ ASSOCIATED CONTENT

Supporting Information

The Supporting Information is available free of charge at https://pubs.acs.org/doi/10.1021/acsbiomaterials.0c00807.

^{1}H and ^{13}C NMR spectra of the synthesized 1-(anthracen-9-ylmethyl)-1H-imidazole and CHO-AIL, HRMS spectrum of CHO-AIL, and influence of pH, sweep rate, and operating potential on the HRP-CHO-AIL/AuNPs/GCE (PDF)

■ AUTHOR INFORMATION

Corresponding Authors

Kathavarayan Thenmozhi − *Department of Chemistry, School of Advanced Sciences, Vellore Institute of Technology (VIT), Vellore 632014, India;* orcid.org/0000-0002-9016-5380; Email: kt.thenmozhi@gmail.com, k.thenmozhi@vit.ac.in

Sellappan Senthilkumar − *Department of Chemistry, School of Advanced Sciences, Vellore Institute of Technology (VIT), Vellore 632014, India;* orcid.org/0000-0002-1770-2442; Email: senthilanalytical@gmail.com, senthilkumar.s@vit.ac.in

Authors

Kandaswamy Theyagarajan − *Department of Chemistry, School of Advanced Sciences, Vellore Institute of Technology (VIT), Vellore 632014, India;* orcid.org/0000-0002-2959-5648

Sangeeta Yadav − *School of Biosciences and Technology and Centre for Nanobiotechnology, Vellore Institute of Technology (VIT), Vellore 632014, India*

Jitendra Satija − *Centre for Nanobiotechnology, Vellore Institute of Technology (VIT), Vellore 632014, India*

Complete contact information is available at: https://pubs.acs.org/10.1021/acsbiomaterials.0c00807

Notes

The authors declare no competing financial interest.

■ ACKNOWLEDGMENTS

Science and Engineering Research Board (SERB), Government of India (sanction no. SB/FT/CS-018/2014), is sincerely acknowledged for financial assistance.

■ REFERENCES

(1) Kimmel, D. W.; LeBlanc, G.; Meschievitz, M. E.; Cliffel, D. E. Electrochemical Sensors and Biosensors. *Anal. Chem.* **2012**, *84*, 685−707.

(2) Salimian, R.; Shahrokhian, S.; Panahi, S. Enhanced Electrochemical Activity of a Hollow Carbon Sphere/Polyaniline-Based Electrochemical Biosensor for HBV DNA Marker Detection. *ACS Biomater. Sci. Eng.* **2019**, *5*, 2587−2594.

(3) Labadi, Z.; Kalas, B.; Saftics, A.; Illes, L.; Jankovics, H.; Bereczk-Tompa, É.; Sebestyén, A.; Tóth, É.; Kakasi, B.; Moldovan, C.; Firtat, B.; Gartner, M.; Gheorghe, M.; Vondervisztt, F.; Fried, M.; Petrik, P. Sensing Layer for Ni Detection in Water Created by Immobilization of Bioengineered Flagellar Nanotubes on Gold Surfaces. *ACS Biomater. Sci. Eng.* **2020**, *6*, 3811−3820.

(4) da Silva, W.; Brett, C. M. A. Novel Biosensor for Acetylcholine Based on Acetylcholinesterase/Poly(Neutral Red) − Deep Eutectic Solvent/Fe_2O_3 Nanoparticle Modified Electrode. *J. Electroanal. Chem.* **2020**, *872*, 114050.

(5) Wang, Z.; Luo, X.; Wan, Q.; Wu, K.; Yang, N. Versatile Matrix for Constructing Enzyme-Based Biosensors. *ACS Appl. Mater. Interfaces* **2014**, *6*, 17296−17305.

(6) Moreau, A. L. D.; Janissen, R.; Santos, C. A.; Peroni, L. A.; Stach-Machado, D. R.; de Souza, A. A.; de Souza, A. P.; Cotta, M. A. Highly-Sensitive and Label-Free Indium Phosphide Biosensor for Early Phytopathogen Diagnosis. *Biosens. Bioelectron.* **2012**, *36*, 62−68.

(7) Zhang, M.; Zheng, J.; Wang, J.; Xu, J.; Hayat, T.; Alharbi, N. S. Direct Electrochemistry of Cytochrome c Immobilized on One Dimensional Au Nanoparticles Functionalized Magnetic N-Doped Carbon Nanotubes and its Application for the Detection of H_2O_2. *Sens. Actuators, B* **2019**, *282*, 85−95.

(8) Liu, X.; Feng, H.; Zhang, J.; Zhao, R.; Liu, X.; Wong, D. K. Y. Hydrogen Peroxide Detection at a Horseradish Peroxidase Biosensor with a Au Nanoparticle-Dotted Titanate NanotubelHydrophobic Ionic Liquid Scaffold. *Biosens. Bioelectron.* **2012**, *32*, 188−194.

(9) Xu, S.; Huang, X.; Chen, Y.; Liu, Y.; Zhao, W.; Sun, Z.; Zhu, Y.; Liu, X.; Wong, C.-P. Silver Nanoparticle-Enzyme Composite Films for Hydrogen Peroxide Detection. *ACS Appl. Nano Mater.* **2019**, *2*, 5910−5921.

(10) Su, S.; Han, X.; Lu, Z.; Liu, W.; Zhu, D.; Chao, J.; Fan, C.; Wang, L.; Song, S.; Weng, L.; Wang, L. Facile Synthesis of a MoS_2-Prussian Blue Nanocube Nanohybrid-Based Electrochemical Sensing Platform for Hydrogen Peroxide and Carcinoembryonic Antigen Detection. *ACS Appl. Mater. Interfaces* **2017**, *9*, 12773−12781.
(11) Sampath, S.; Lev, O. Renewable, Reagentless Glucose Sensor Based on a Redox Modified Enzyme and Carbon-Silica Composite. *Electroanalysis* **1996**, *8*, 1112−1116.
(12) Kang, X. B.; Pang, G. C.; Liang, X. Y.; Wang, M.; Liu, J.; Zhu, W. M. Study on a Hydrogen Peroxide Biosensor Based on Horseradish Peroxidase/GNPs-Thionine/Chitosan. *Electrochim. Acta* **2012**, *62*, 327−334.
(13) Rengan, A. K.; Jagtap, M.; De, A.; Banerjee, R.; Srivastava, R. Multifunctional Gold Coated Thermo-Sensitive Liposomes for Multimodal Imaging and Photo-Thermal Therapy of Breast Cancer Cells. *Nanoscale* **2014**, *6*, 916−923.
(14) Li, T.; Li, F.; Xiang, W.; Yi, Y.; Chen, Y.; Cheng, L.; Liu, Z.; Xu, H. Selenium-Containing Amphiphiles Reduced and Stabilized Gold Nanoparticles: Kill Cancer Cells via Reactive Oxygen Species. *ACS Appl. Mater. Interfaces* **2016**, *8*, 22106−22112.
(15) Senthil kumar, S.; Kwak, K.; Lee, D. Electrochemical Sensing using Quantum-Sized Gold Nanoparticles. *Anal. Chem.* **2011**, *83*, 3244−3247.
(16) Huo, X.; Liu, X.; Liu, J.; Sukumaran, P.; Alwarappan, S.; Wong, D. K. Y. Strategic Applications of Nanomaterials as Sensing Platforms and Signal Amplification Markers at Electrochemical Immunosensors. *Electroanalysis* **2016**, *28*, 1730−1749.
(17) Zhang, T.; Wang, W.; Zhang, D.; Zhang, X.; Ma, Y.; Zhou, Y.; Qi, L. Biotemplated Synthesis of Gold Nanoparticle-Bacteria Cellulose Nanofiber Nanocomposites and Their Application in Biosensing. *Adv. Funct. Mater.* **2010**, *20*, 1152−1160.
(18) Tanner, E. E. L.; Piston, K. M.; Ma, H.; Ibsen, K. N.; Nangia, S.; Mitragotri, S. The Influence of Water on Choline-Based Ionic Liquids. *ACS Biomater. Sci. Eng.* **2019**, *5*, 3645−3653.
(19) Damlin, P.; Suominen, M.; Heinonen, M.; Kvarnström, C. Non-Covalent Modification of Graphene Sheets in PEDOT Composite Materials by Ionic Liquids. *Carbon* **2015**, *93*, 533−543.
(20) Dias, A. M. A.; Cortez, A. R.; Barsan, M. M.; Santos, J. B.; Brett, C. M. A.; De Sousa, H. C. Development of Greener Multi-responsive Chitosan Biomaterials Doped with Biocompatible Ammonium Ionic Liquids. *ACS Sustainable Chem. Eng.* **2013**, *1*, 1480−1492.
(21) Qin, Y.; Song, Y.; Sun, N.; Zhao, N.; Li, M.; Qi, L. Ionic Liquid-Assisted Growth of Single-Crystalline Dendritic Gold Nanostructures with a Three-Fold Symmetry. *Chem. Mater.* **2008**, *20*, 3965−3972.
(22) Theyagarajan, K.; Saravanakumar, D.; Senthilkumar, S.; Thenmozhi, K. Rationally Designed Naphthyl Substituted Amine Functionalized Ionic Liquid Platform for Covalent Immobilization and Direct Electrochemistry of Hemoglobin. *Sci. Rep.* **2019**, *9*, 10428.
(23) Murphy, M.; Theyagarajan, K.; Ganesan, P.; Senthilkumar, S.; Thenmozhi, K. Electrochemical Biosensor for The Detection of Hydrogen Peroxide Using Cytochrome C Covalently Immobilized on Carboxyl Functionalized Ionic Liquid/Multiwalled Carbon Nanotube Hybrid. *Appl. Surf. Sci.* **2019**, *492*, 718−725.
(24) Opallo, M.; Lesniewski, A. A Review on Electrodes Modified with Ionic Liquids. *J. Electroanal. Chem.* **2011**, *656*, 2−16.
(25) Zheng, Z.; Guo, J.; Mao, H.; Xu, Q.; Qin, J.; Yan, F. Metal-Containing Poly(Ionic Liquid) Membranes for Antibacterial Applications. *ACS Biomater. Sci. Eng.* **2017**, *3*, 922−928.
(26) Manoj, D.; Theyagarajan, K.; Saravanakumar, D.; Senthilkumar, S.; Thenmozhi, K. Aldehyde Functionalized Ionic Liquid on Electrochemically Reduced Graphene Oxide as a Versatile Platform for Covalent Immobilization of Biomolecules and Biosensing. *Biosens. Bioelectron.* **2018**, *103*, 104−112.
(27) Wang, Z.; Li, M.; Su, P.; Zhang, Y.; Shen, Y.; Han, D.; Ivaska, A.; Niu, L. Direct Electron Transfer of Horseradish Peroxidase and Its Electrocatalysis Based on Carbon Nanotube/Thionine/Gold Composites. *Electrochem. Commun.* **2008**, *10*, 306−310.
(28) Teng, Y. J.; Zuo, S. H.; Lan, M. B. Direct Electron Transfer of Horseradish Peroxidase on Porous Structure of Screen-Printed Electrode. *Biosens. Bioelectron.* **2009**, *24*, 1353−1357.
(29) Chen, W.; Cai, S.; Ren, Q.-Q.; Wen, W.; Zhao, Y.-D. Recent Advances in Electrochemical Sensing for Hydrogen Peroxide: A Review. *Analyst* **2012**, *137*, 49−58.
(30) Fang, R.; Xu, H.; Cao, W.; Yang, L.; Zhang, X. Reactive Oxygen Species (ROS)-Responsive Tellurium-Containing Hyperbranched Polymer. *Polym. Chem.* **2015**, *6*, 2817−2821.
(31) Sarkar, A.; Ghosh, A. B.; Saha, N.; Bhadu, G. R.; Adhikary, B. Newly Designed Amperometric Biosensor for Hydrogen Peroxide and Glucose Based on Vanadium Sulfide Nanoparticles. *ACS Appl. Nano Mater.* **2018**, *1*, 1339−1347.
(32) Chen, S.; Yuan, R.; Chai, Y.; Hu, F. Electrochemical Sensing of Hydrogen Peroxide Using Metal Nanoparticles: A Review. *Microchim. Acta* **2013**, *180*, 15−32.
(33) Satija, J.; Punjabi, N. S.; Sai, V. V. R.; Mukherji, S. Optimal Design for U-Bent Fiber-Optic LSPR Sensor Probes. *Plasmonics* **2014**, *9*, 251−260.
(34) Munro, C. H.; Smith, W. E.; Garner, M.; Clarkson, J.; White, P. C. Characterization of the Surface of a Citrate-Reduced Colloid Optimized for Use as a Substrate for Surface-Enhanced Resonance Raman Scattering. *Langmuir* **1995**, *11*, 3712−3720.
(35) Jain, P. K.; Lee, K. S.; El-Sayed, I. H.; El-Sayed, M. A. Calculated Absorption and Scattering Properties of Gold Nanoparticles of Different Size, Shape, and Composition: Applications in Biological Imaging and Biomedicine. *J. Phys. Chem. B* **2006**, *110*, 7238−7248.
(36) Mandegani, Z.; Asadi, Z.; Asadi, M.; Karbalaei-Heidari, H. R.; Rastegari, B. Synthesis, Characterization, DNA Binding, Cleavage Activity, Cytotoxicity and Molecular Docking of New Nano Water-Soluble $[M(5\text{-}CH_2PPh_3\text{-}3,4\text{-salpyr})](ClO_4)_2$ (M = Ni, Zn) Complexes. *Dalton Trans.* **2016**, *45*, 6592−6611.
(37) Benjamin, M.; Manoj, D.; Thenmozhi, K.; Bhagat, P. R.; Saravanakumar, D.; Senthilkumar, S. A Bioinspired Ionic Liquid Tagged Cobalt-Salophen Complex for Nonenzymatic Detection of Glucose. *Biosens. Bioelectron.* **2017**, *91*, 380−387.
(38) Thenmozhi, K.; Narayanan, S. S. Horseradish Peroxidase and Toluidine Blue Covalently Immobilized Leak-Free Sol-Gel Composite Biosensor for Hydrogen Peroxide. *Mater. Sci. Eng., C* **2017**, *70*, 223−230.
(39) Bonanni, A.; Pumera, M.; Miyahara, Y. Influence of Gold Nanoparticle Size (2-50 nm) upon Its Electrochemical Behavior: An Electrochemical Impedance Spectroscopic and Voltammetric Study. *Phys. Chem. Chem. Phys.* **2011**, *13*, 4980−4986.
(40) Zhang, H.-L.; Zou, X.-Z.; Lai, G.-S.; Han, D.-Y.; Wang, F. Direct Electrochemistry of Hemoglobin Immobilized on Carbon-Coated Iron Nanoparticles for Amperometric Detection of Hydrogen Peroxide. *Electroanalysis* **2007**, *19*, 1869−1874.
(41) Carlin, R. T.; Truelove, P. C.; Osteryoung, R. A. Electrochemical and spectroscopic study of anthracene in a mixed Lewis-Brønsted acid ambient temperature molten salt system. *Electrochim. Acta* **1992**, *37*, 2615−2628.
(42) Cheng, E.; Sun, T.-C.; Oliver Su, Y. Electrochemical Reduction of Substituted Anthracenes. *J. Chin. Chem. Soc.* **1993**, *40*, 551−555.
(43) Koposova, E.; Liu, X.; Kisner, A.; Ermolenko, Y.; Shumilova, G.; Offenhäusser, A.; Mourzina, Y. Bioelectrochemical Systems with Oleylamine-Stabilized Gold Nanostructures and Horseradish Peroxidase for Hydrogen Peroxide Sensor. *Biosens. Bioelectron.* **2014**, *57*, 54−58.
(44) Vusa, C. S. R.; Manju, V.; Berchmans, S.; Arumugam, P. Electrochemical Amination of Graphene Using Nanosized PAMAM Dendrimers for Sensing Applications. *RSC Adv.* **2016**, *6*, 33409−33418.
(45) Xu, X.; Yan, S.; Wang, B.; Qu, P.; Wang, J.; Wu, J. Graphene Aerogel/Platinum Nanoparticle Nanocomposites for Direct Electrochemistry of Cytochrome c and Hydrogen Peroxide Sensing. *J. Nanosci. Nanotechnol.* **2016**, *16*, 12299−12306.

https://dx.doi.org/10.1021/acsbiomaterials.0c00807
ACS Biomater. Sci. Eng. XXXX, XXX, XXX−XXX

(46) Baccarin, M.; Janegitz, B. C.; Berté, R.; Vicentini, F. C.; Banks, C. E.; Fatibello-Filho, O.; Zucolotto, V. Direct Electrochemistry of Hemoglobin and Biosensing for Hydrogen Peroxide Using a Film Containing Silver Nanoparticles and Poly(Amidoamine) Dendrimer. *Mater. Sci. Eng., C* **2016**, *58*, 97−102.
(47) Yuan, J.; Xu, S.; Zeng, H.-Y.; Cao, X.; Dan Pan, A.; Xiao, G.-F.; Ding, P.-X. Hydrogen Peroxide Biosensor Based on Chitosan/2D Layered Double Hydroxide Composite for The Determination of H_2O_2. *Bioelectrochemistry* **2018**, *123*, 94−102.
(48) Gautam, V.; Singh, K. P.; Yadav, V. L. Polyaniline/Multiwall Carbon Nanotubes/Starch Nanocomposite Material and Hemoglobin Modified Carbon Paste Electrode for Hydrogen Peroxide and Glucose Biosensing. *Int. J. Biol. Macromol.* **2018**, *111*, 1124−1132.
(49) dos Santos Pereira, T.; Mauruto de Oliveira, G. C.; Santos, F. A.; Raymundo-Pereira, P. A.; Oliveira, O. N.; Janegitz, B. C. Use of Zein Microspheres to Anchor Carbon Black and Hemoglobin in Electrochemical Biosensors to Detect Hydrogen Peroxide in Cosmetic Products, Food and Biological Fluids. *Talanta* **2019**, *194*, 737−744.

https://dx.doi.org/10.1021/acsbiomaterials.0c00807
ACS Biomater. Sci. Eng. XXXX, XXX, XXX−XXX